Received: 30 November 2024 | Revised: 24 March 2025 | Accepted: 18 June 2025 | Published online: 9 July 2025

RESEARCH ARTICLE

Journal of Optics and Photonics Research
2025, Vol. 00(00) 1–12
DOI: 10.47852/bonviewJOPR52024929

BON VIEW PUBLISHING

Deep Learning Model-Based Adaptive Power Transfer in FSO Communications

Wen-Yao Liu[1], Yan-Qing Hong[1,*], Xu Liu[1], Xue-Heng Chen[1] and Peng-Fei Lv[1]

[1]*School of Information Science and Engineering, Shenyang University of Technology, China*

Abstract: In bidirectional atmospheric channel transmission with channel reciprocity, the correlation between two transmission channel turbulence noises is high, and different techniques can be used to extract channel state information (CSI) in forward transmission, and adaptive power techniques can be used to inhibit turbulence effects in reverse transmission to improve the performance of free-space optical (FSO) systems. In atmospheric FSO communication systems, the scintillation response from turbulence effects increases the bit error rate (BER) of the communication system and reduces the system performance. In this paper, we propose two different adaptive power transmission (APT) techniques, namely gated recurrent unit (GRU)-based APT with cascading LPF and recurrent neural network (RNN)-based APT with cascading LPF, which utilizes the CSI of the channel for adaptive transmission to reduce BER. The proposed adaptive power transfer technique can improve the BER performance of the system and effectively mitigate the scintillation effect caused by atmospheric turbulence on the FSO communication system. A bidirectional atmospheric channel with different turbulence intensities is constructed in the simulation software, different background noises are added to change the channel reciprocity, the effect of reciprocity on the signal transmission is investigated, and the performance of different deep learning models in bidirectional channels. The future development of the technique is promising. According to the simulation results, APT technology based on deep learning achieves a lower bound that stabilizes at 10^{-4}∼10^{-5} in turbulent channels under high signal-to-noise ratio conditions. Specifically, the LPF-RNN-APT technology excels due to its lightweight structure and parameter efficiency, delivering outstanding performance in strongly symmetric channels.

Keywords: free-space optical communications, channel reciprocity, channel state information, adaptive power transmission

1. Introduction

Free-space optical communication (FSO) is a technology that utilizes optical signals for information transmission in free space. The primary benefits of FSO communication are that it can satisfy the demands of contemporary data-intensive applications due to its very fast data transfer rate and greater data bandwidth than traditional radio communications [1]. FSO is also especially well-suited for usage in calm settings due to its interference-free nature, as optical signals do not interact with other frequency bands [2]. Installing and deploying FSO systems is rather easy, particularly when it comes to transmitting in the visible and near-infrared spectrum. There are several drawbacks to FSO communication despite all of its benefits [3]. One major factor affecting the quality of signal transmission, which can result in signal distortion and attenuation, is atmospheric turbulence [4]. Rain, snow, and haze are examples of weather conditions that can have a significant impact on optical signal transmission. Large or moving obstructions may disrupt the optical alignment of the FSO system, which in turn may impact the transmission's overall dependability [5]. FSO may be made more reliable and effective by offsetting these negative impacts.

To overcome the effects brought about by atmospheric turbulence, researchers have proposed various compensation techniques. Maalej and Besbes [6] explore the performance of FSO communication systems based on dual generalized gamma channels with M-ary PPM modulation. This approach is able to reduce the resulting noise to some extent by choosing the appropriate modulation. Meanwhile, the design and optimization of the optical receiver is also one of the important means to improve the system's performance. Adaptive techniques also show great potential in this regard. By dynamically adjusting the transmission parameters (e.g., power and modulation form), adaptive transmission systems are able to effectively improve the quality of signals under unfavorable conditions [7]. For example, Hufnagel et al. [8] have investigated underwater channels in quantum communications to provide different technical solutions for signal compensation. APT technology is an important development direction in FSO communication research. Adaptive technology can dynamically adjust the signal strength according to the current environmental conditions and channel state, so as to realize the best performance in different operating environments [9]. For example, Liu et al. [10] propose a reciprocity-based adaptive power transfer strategy in two-way atmospheric channels. This approach utilizes channel state information (CSI) to be able to adjust the power delivery in a timely manner when the environment changes, improving the robustness of the system.

In recent years, the application of deep learning techniques in the field of communication has received increasing attention [11]. Deep learning can be used not only for signal processing and feature extraction but also for intelligent adaptive system design. Padhy and Patnaik [12] propose a deep learning-based channel estimator that operates without requiring pilot sequences, demonstrating the advantages of deep

*Corresponding author: Yan-Qing Hong, School of Information Science and Engineering, Shenyang University of Technology, China. Email: hongy7@sut.edu.cn

learning in signal classification and adaptive decision-making. Combining deep learning and adaptive transmission techniques enables the system to make more accurate decisions based on real-time data [13]. Specifically, deep learning can predict channel conditions by analyzing historical transmission data and adjusting transmission parameters accordingly [14]. For example, Amirabadi et al. [15] investigate the effect of deep learning on channel estimation in FSO communication systems, showing good performance improvement. In two-way atmospheric channels, techniques for reciprocity-based adaptive transmission via deep learning are gaining more and more attention [16]. However, the research faces many challenges, such as atmospheric turbulence and weather effects, through which problems are yet to be solved [17, 18].

In this paper, in order to mitigate the impact of the scintillation effect, it is proposed to use two different deep learning model-based APT techniques in bidirectional atmospheric channels and combine them with a low-pass filter; the two adaptive transmission techniques are gated recurrent unit-based adaptive power transmission (APT) with cascading LPF (LPF-GRU-APT) and recurrent neural network (RNN)-based APT with cascading LPF (LPF-RNN-APT). In the reciprocity-based FSO system, the forward transmitting receiver side uses different techniques for CSI estimation of the signal and APT based on known CSI in the transmitter side of the reverse transmission to reduce the bit error rate (BER) of the transmitted signal. More precisely, the primary focus of this paper can be summarized as follows.

1) In the study of turbulent channels based on reciprocity, we integrate deep learning with adaptive transmission techniques and propose two novel transmission technologies: the LPF-GRU-APT and the LPF-RNN-APT. Reduce the impact of fading effects on signal and improve the system's transmission performance. This study investigates the compatibility of various deep learning models with reciprocal channels.
2) Furthermore, this paper presents a modeling study of bidirectional atmospheric channels, comprehensively considering various influencing factors such as background noise and signal decay. A turbulent channel model incorporating three typical fading coefficients is established, and the performance and adaptability of the deep learning-based APT technology under different channel conditions are analyzed in depth.
3) Finally, this paper replicates the traditional fixed threshold decision (FTD) and adaptive transmission decision (ATD) techniques, as well as an APT technology that employs a cascaded LPF to extract CSI in reciprocal channels, for the purpose of comparison. This allows for a more intuitive and convenient observation of the transmission performance of the proposed deep learning-based APT technology.

2. Turbulence Channel Analysis

Two transceivers, designated as a and b, are assigned to capture a signal transmitted through a bidirectional optical wireless channel, which is affected by air turbulence, as outlined in the bidirectional atmospheric propagation model employed in this study. The two transceivers a and b are located at the same end of the link. The transceivers located at the two ends of the link with the same axis symmetry can complete the transmission process of transmit-receive-transmit in a short time, which is schematically shown in Figure 1. We refer to beam waves propagating from the transmission that occurs in both directions, from point A to point B and vice versa, as a form of forward transmission and reverse transmission beam waves, respectively [10, 19]. The forward transmission process consists of the modulation of the On-Off

Figure 1
Block diagram of the bidirectional atmospheric channel model

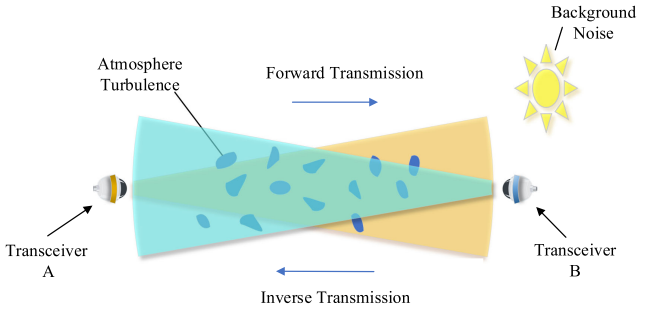

Keying (OOK) signal by transceiver a and the emission of beam s(t), which is transmitted through a turbulent channel to transceiver b. The intensity of the scintillation effect due to atmospheric turbulence of the signal is evaluated by the scintillation index [20]:

$$\sigma^2 = \langle I^2 \rangle / \langle I^2 \rangle - 1 \tag{1}$$

where <·> indicates the ensemble average and I represents the light intensity of the received OOK signal. Utilizing an analog-to-digital converter (ADC), the transceiver b at the receiving end transforms the received optical signal into an electrical signal, which is then transformed into a digital signal $r[k]$ and represented as [21]:

$$r[k] = I[k]s[k] + n[k] \tag{2}$$

where $I[k]$ denotes intensity fluctuations, $s[k]$ is the transmitted signal and $n[k]$ denotes additive Gaussian white noise (AWGN). The reverse transmission is the same. Under ideal conditions, a reciprocity-based FSO system can achieve $h_{ab}(t) = h_{ba}(t)$, meaning the channel responses in the time domain are identical for both transmission directions [22]. This allows the extraction of channel information from the forward transmission signal to enhance the performance of the reverse transmission [23]. However, due to factors such as laser wavelength shift, nonlinear response of photodetectors, and atmospheric scattering, the two channels cannot be completely identical in practice. The reciprocity ρ between the two transmissions can be quantified using a correlation coefficient [24]:

$$\rho = \frac{cov(I_F, I_R)}{\sigma_F \sigma_R} = \frac{E[I_F I_R] - 1}{\sqrt{(1+\sigma_F^2)(1+\sigma_R^2)}} \tag{3}$$

where the subscripts F and R stand for forward transmission and reverse transmission, respectively, the function $cov(\cdot)$ denotes the covariance operation, and $E[\cdot]$ denotes the mathematical variance operation. When the reciprocity parameter ρ approaches 1, the system is in an ideal state; however, under outdoor turbulent conditions, $\rho < 0.99$, resulting in partial loss of reciprocity. The atmospheric turbulence channel of the simulated channel applied in this paper is approximately normally distributed [25], the correlation coefficient and scintillation index may undergo re-assessment [26].

$$\tilde{\rho} = \frac{log(1+\rho\sigma^2)}{log(1+\sigma^2)} \tag{4}$$

3. Operation Principle

The system block diagram illustrating the APT methodology introduced in this paper is presented in Figure 2. The goal of

Figure 2
System block diagram of adaptive power transfer technique: (a) LPF-based APT, (b) LPF-GRU-APT, and (c) LPF-RNN-APT APT

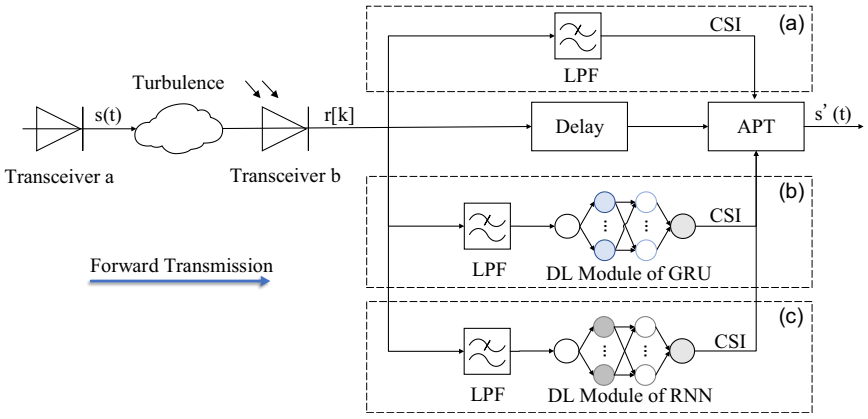

suppressing turbulence and improving communication quality in a bidirectional atmospheric channel can be accomplished by extracting the CSI of the forward transmission pathway and adjusting the signal power based on the known CSI in the reverse transmission. This is possible because the turbulence intensity of the forward transmission and reverse transmission channels is related. The detailed procedure is outlined as follows: at the transmission source of the forward link, an amplitude of either 0 or 1 is produced, followed by a sequence of pulses, which are then transmitted through the turbulent channel subsequent to OOK modulation. At the receiving end, the signal is divided into two paths: one path is used to estimate the channel attenuation characteristics based on the intensity variations of the received signal and the other way is to wait for the CSI for adaptive adjustment. At this stage, the endpoint designated for forward transmission transitions to serve as the endpoint for reverse transmission. Utilizing the known CSI, the OOK signal strength is modulated, exhibiting increased power levels at lower channel quality and reduced power levels at higher quality scenarios. The transceiver captures the signal at the reverse transmission endpoint, conducts an additional CSI assessment, and subsequently relays the findings back. To enhance communication quality, this approach facilitates a closed-loop control system that enables the dynamic adjustment of broadcast signal strength in accordance with the actual communication conditions. In this study, we execute adaptive power transfer and extract CSI using a new method.

3.1. The principles of FTD, ATD, and APT based on LPF

For APT technology, the most crucial element is accurate CSI, which involves the real-time acquisition and precise estimation of key parameters such as channel attenuation, multipath effects, and noise. This is the core for achieving high-efficiency and low-energy-consumption communication. The APT technology based on threshold decision makes judgments on the signal quality by directly utilizing the received signal strength, in combination with both fixed and adaptive thresholds, and thus dynamically adjusts the transmission power. Among them, FTD technology employs a pre-set power threshold to implement power control in a simple and real-time manner as shown in Figure 3(a). In contrast, the ATD technology adjusts the threshold according to the dynamic changes in the receiving environment, achieving more flexible power adaptation as shown in Figure 3(b). While FTD is straightforward and easy to implement, it has limited adaptability to dynamic environmental changes. On the other hand, ATD offers better adaptability to complex environments, though it involves higher algorithmic complexity.

Bidirectional reciprocity implies that the uplink and downlink channels are symmetric, meaning it may only be necessary to estimate the CSI in one direction, with the other direction inferred through reciprocity. However, in practice, non-ideal factors such as hardware differences and environmental variations can lead to

Figure 3
Schematic diagram of decision technology: (a) FTD and (b) ATD

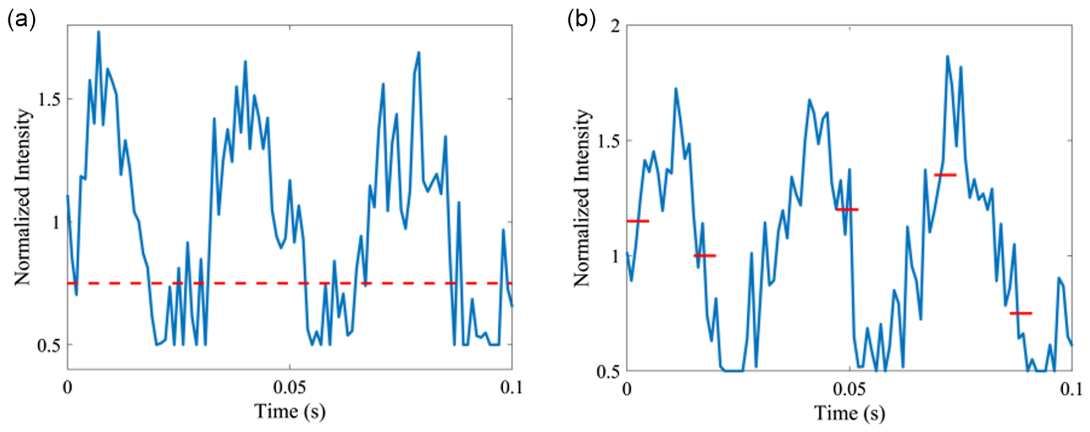

incomplete reciprocity. The LPF plays a crucial role in addressing these real-world noises. It suppresses high-frequency random noise, making the estimated CSI closer to its true value and thereby improving power control. Additionally, the LPF reduces errors caused by short-term fluctuations, particularly in FSO systems where rapid changes are induced by atmospheric turbulence. In Figure 2(a), adding low-pass filtering to extract the CSI can obtain a more stable channel state estimation, which makes the power adjustment more robust and improves the system's ability to adapt to environmental changes, and thus can better ensure the reliability of the communication.

During the forward transmission process, the optical signal captured by transceiver B initiates an important conversion from the optical domain to the electrical domain. This optical signal is connected to an ADC. The ADC, set at a specific sampling frequency, precisely transforms the continuously varying analog optical signal into a discrete digital signal, thus completing the transformation of the signal form to make it conform to the subsequent processing requirements based on digital logic. After that, the signal passes through the low-pass filter, and the output signal $\hat{r}[k]$ can be expressed as:

$$\hat{r}[k] = r[k]h_L[k] = \sum r[n]h_L[k-n] \tag{5}$$

Among them, $h_L[k]$ is the impulse response of the filter, $\sum$ represents the summation symbol, and n is the index representing the discrete-time sequence. The frequency components of the received signal are calculated using the discrete Fourier transform, and the calculation formula is as follows [27]:

$$D(f) = \sum_{n=0}^{N-1} \hat{r}[k] \cdot e^{(-j2\pi fn/N)} \tag{6}$$

where N is the signal length, n represents a specific moment in the temporal domain, and $D(f)$ is the discrete Fourier transform of the output signal $r[k]$. Then, the power spectral density (PSD) is used to calculate the frequency characteristics of the received signal, and the formula is as follows [28]:

$$S(f) = \frac{1}{N}|D(f)|^2 \tag{7}$$

Based on the time-domain and frequency-domain information of the signal that has passed through the low-pass filter, the state of the channel information within the channel can be understood. Subsequently, power control can be carried out to improve the BER performance.

3.2. APT based on LPF and GRU

In the field of deep learning, the combination of the GRU model and the APT technology can significantly enhance the performance of communication systems. By conducting sequential modeling of historical signal data, the GRU model can more accurately predict the CSI, thus optimizing the power transmission strategy. Its powerful ability to handle sequential dependencies enables it to perform exceptionally well in capturing dynamic changes such as channel attenuation, multipath effects, and noise. Through real-time adjustment of the transmission power, the GRU model can remarkably improve the accuracy of CSI estimation, reduce channel estimation errors, and thereby achieve more efficient and reliable APT, ultimately enhancing the overall performance of the communication system. After the signal passes through the low-pass filter, the GRU model, which has a simplified structure and can efficiently capture long-sequence dependencies, is selected to receive the signal from which the high-frequency noise has been removed. The mathematical formula for its internal hidden state can be expressed as:

$$\begin{aligned} r[k] &= \sigma(W_r \cdot \hat{r}[k] + U_r \cdot h[k-1] + b_r) \\ z[k] &= \sigma(W_z \cdot \hat{r}[k] + U_z \cdot h[k-1] + b_z) \\ h[k] &= (1 - z[k]) \circ h[k-1] + z[k] \\ &\quad \circ tanh(W_h \cdot \hat{r}[k] + U_h \cdot h[k-1] + b_h) \end{aligned} \tag{8}$$

Among them, σ only represents the sigmoid function, $\circ$ represents element-wise multiplication, $r[k]$ only represents the reset gate, $z[k]$ is the update gate. W_r, W_z, W_h are weight matrices, U_r, U_z, U_h denote the recurrent weight matrices, and b_r, b_z, b_h are bias vectors. However, to adapt to the bidirectional channel, a Batch Normalization (BN) layer and a rectified linear unit (ReLU) layer are incorporated into the GRU model. The normalization layer normalizes the output of the GRU, alleviating the problem of gradient vanishing in the inner layers and accelerating the training process:

$$\begin{aligned} \mu[k] &= \frac{1}{m}\sum_{i=1}^{m} h[k]^{(i)} \\ \sigma^2[k] &= \frac{1}{m}\sum_{i=1}^{m} (h[k]^{(i)} - \mu[k])^2 \\ BN(h[k]) &= \gamma \cdot \frac{h[k] - \mu[k]}{\sqrt{\sigma^2[k] + \varepsilon}} + \beta \end{aligned} \tag{9}$$

Among them, γ and β only represents the sigmoid function, ε is a small constant to avoid a zero denominator. The ReLU activation function performs a non-linear mapping on the output of the BN layer, enhancing the model's expressive ability.

$$a[k] = ReLU(BN(h[k])) = max(0, BN(h[k])) \tag{10}$$

After the input signal is preprocessed, the GRU network processes the data at each time step by step. It dynamically adjusts the information flow through the update gate and reset gate mechanisms to extract sequential features. The Adam optimizer is used to train the model, which adaptively adjusts the learning rate of parameters. The number of training epochs is set to 40, and the batch size is set to 8 to ensure the stable optimization of the model. The signal is input into the trained GRU model, and the model's sequence modeling ability is utilized to analyze the signal. The CSI values are output and subjected to binarization processing to clearly reflect the channel state. Eventually, the estimated CSI value is obtained, and APT is carried out according to this value. Table 1 shows the layer structure of the GRU model used.

Table 1
GRU network model structure parameters

Number	Type	Parameter
1	Sequence Input	Size(train_put,1)
2	GRU	Neuron：64
3	RN	\
4	ReLU	\
5	Fully Connected	1
6	Regression	\

3.3. APT based on LPF and RNN

As shown in Figure 2(c), the OOK signal $r[k]$ is evenly divided into upper and lower branches. The lower branch is used to obtain the real-time CSI of the turbulent channel, as the turbulent channel has the characteristic of being dominated by low frequencies. In addition, the intensity of the CSI signal extracted through the low-pass filter is approximately half of that of the signal before being filtered by the low-pass filter. Therefore, the extracted CSI signal is directly used as the decision threshold for the OOK signal detected by the lower branch. The delay is used to match the synchronization between the signals of the upper and lower branches. Through the low-pass filter, the low-frequency CSI components can be more effectively extracted from the received OOK signal. After the signal passes through the low-pass filter, the input layer of the RNN model receives the signal $\hat{r}[k]$ from which the high-frequency noise has been removed, and then processes the sequential signal:

$$f_k = \sigma\left(W_f \cdot \hat{r}[k] + U_f \cdot h[k-1] + b_f\right)$$

$$i_k = \sigma(W_i \cdot \hat{r}[k] + U_i \cdot h[k-1] + b_i)$$

$$c_k = f_k \circ c[k-1] + i_k \circ tanh(W_c \cdot \hat{r}[k] + U_c \cdot h[k-1] + b_c)$$

$$o_k = \sigma(W_o \cdot \hat{r}[k] + U_o \cdot h[k-1] + b_o)$$

$$h[k] = o_k \circ tanh(c_k) \tag{11}$$

W are weight matrices, U denote the recurrent weight matrices, and b are bias vectors. It should be noted again that in the deep learning model, σ represents the sigmoid function. In the RNN model as given in Figure 4, the output layer maps the hidden state, which can be expressed as:

$$\hat{h}[k] = W_{out} \cdot h[k] + b_{out} \tag{12}$$

After the input signal is preprocessed, the hidden layer processes the data at each time step by step. By utilizing memory cells and gating mechanisms, it remembers long-term dependencies and extracts sequential features that are helpful for CSI prediction. The RNN model is trained with the input data to optimize the CSI prediction. If the predicted CSI is $g[k]$, then through binarization, the predicted CSI value obtained is:

Figure 4
RNN deep learning model

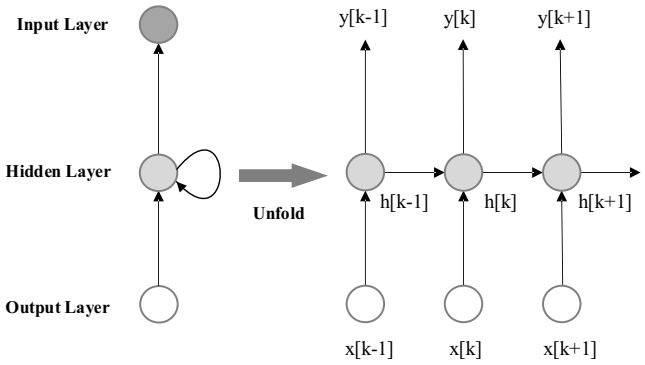

$$\hat{g}_{binary}[k] = \begin{cases} 1 & if\ \hat{g}[k] > threshold \\ 0 & else \end{cases} \tag{13}$$

The temporal sequence processing capabilities and memory functions of RNN models enable them to effectively capture the channel's time-varying and nonlinear characteristics, providing high-precision CSI estimation. Additionally, RNNs can maintain stable performance in complex environments, and when combined with reciprocity, they can further enhance the accuracy of the estimation and improve the overall performance of communication systems.

4. Simulations and Results

In this study, we examine the degradation in performance of FSO systems caused by scintillation phenomena, wherein the probability density function (PDF) of light intensity fluctuations follows a log-normal distribution under conditions of mild atmospheric turbulence. The mathematical representation of its PDF is provided [29]:

$$f(I) = \frac{1}{I\sqrt{2\pi\sigma^2}} exp\left[-\frac{(ln(I) - \mu_I)^2}{2\sigma^2}\right] \tag{14}$$

where I is the signal received strength, μ_I is the mean value, and σ^2 is the log intensity variance. In this paper, the atmospheric channel is represented with the parameters shown in Table 2, and Figure 5 shows the turbulence channel model simulated at $\sigma^2 = 0.0596$. The model allows for a more intuitive display of the attenuation and interference experienced by optical signals. Figure 5(a) shows the PSD in the frequency domain where the predominant low-frequency component, and the PDF of the simulated turbulent channel is shown in Figure 5(b).

In FSO communication systems, the BER is and a classic measure of system performance. BER will also be used in this study to measure the impact of turbulence compensation techniques on the overall system performance. The formula for BER can be expressed as follows [30]:

$$BER = \frac{1}{2}\left[\frac{1}{2} erfc\left(\frac{I_{th}}{\sqrt{2\sigma^2}}\right) + \int_0^{\infty} \frac{1}{2} erfc\left(\frac{I - I_{th}}{\sqrt{2\sigma^2}}\right) f(I) dI\right] \tag{15}$$

In FSO communication system simulation engineering, the noise generated by photodetectors can be modeled as AWGN, and its noise magnitude is measured by signal-to-noise ratio (SNR). While forward and reverse transmissions in two-way atmospheric channels have different effects on the transmission channel due to their different heights and different reception directions, the background noise also has various impacts on the route of transmission. The background noise N_b is measured by SNR, when the effective power of the signal is certain, the smaller the noise power is, the larger N_b is. The SNR can be articulated

Table 2
GRU network model structure parameters

Parameters	Value
Link distance	10 km
Wavelength	1550 nm
C_n^2	2.5×10^{-13}
Aperture	10 cm
Wind speed	5 m/s
Divergence angle	10 urad
Visibility	30 km

Figure 5
Turbulent channel modeling: (a) frequency-domain power spectral density and (b) probability density function

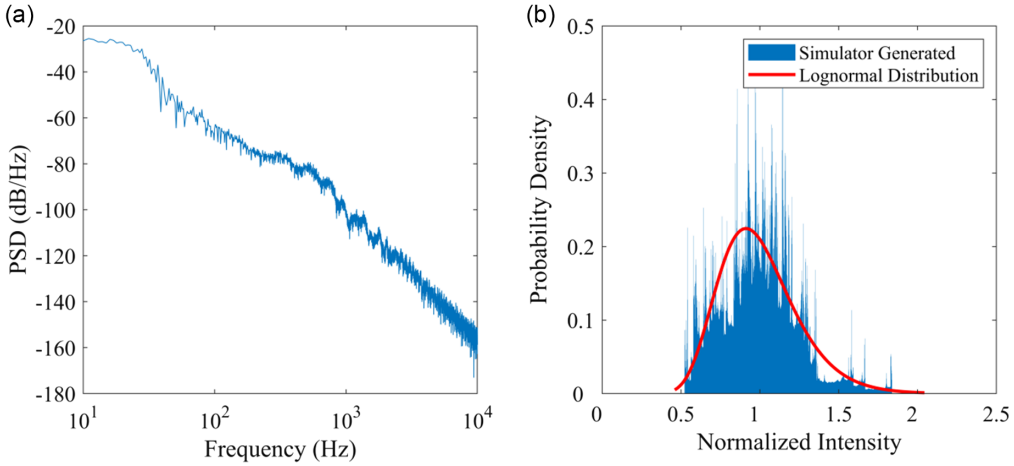

through Equation (16), in which P_s and P_n denote the effective power levels of the signal and the noise, respectively.

$$SNR = 10lg\left(\frac{P_s}{P_n}\right) \tag{16}$$

The reciprocity of the turbulence channel and the received signal's BER of forward transmission and reverse transmission are analyzed in six scenarios where there is a wide range of background noise $N_b = 30$ dB, $N_b = 25$ dB, $N_b = 20$ dB, $N_b = 15$ dB, $N_b = 10$ dB and $N_b = 05$ dB in order to examine the impact of background noise on the two-way channel reciprocity adaptive technique. To facilitate the turbulence channel accessible to comprehend with various background noises, the turbulence channel at a scintillation coefficient of $\sigma^2 = 0.1002$ turbulence channel is utilized as an illustration. The performance of the signal traveling via the channel in the time domain when different background noises are added to this turbulent channel is shown in Figure 6. Figure 6(a)–(d) shows that when noise is added, the time-domain curves are distorted, and as the proportion of noise added increases, the distortion of the signal becomes more and more serious, and the channel reciprocity gradually decreases. However, in the case of adding noise as shown in Figure 6(e) and (f), the channel has almost been flooded by noise and the channel reciprocity is low. In this case, it is difficult to transmit signals with efficient anti-noise techniques under the influence of noise.

The simulation software used in this experiment is MATLAB, the proposed two adaptive power transfer techniques will be tested under three different turbulence intensities with channel models with scintillation indices of 0.0596, 0.1002, and 0.2080, and the system performance of the models is analyzed under the three turbulent channels. The conventional FTD, ATD technique, and LPF-based APT technique are reproduced as a side-by-side comparison. Table 3 lists the primary parameters of the experiment, with the RNN and GRU models operating under identical experimental conditions. Throughout the training process configured as Table 4, the digital signals obtained from the ADC conversion of the received signals at the receiver end will serve as the dataset. Among these, 80% of the dataset is used for training, and 20% is used for testing.

Figure 7 shows the performance of the four communication techniques in the turbulent case of $\sigma^2 = 0.0596$. It is evident that the performance has improved at $\rho > 0.8$, i.e., at three conditions where the background noise is $N_b = 30$ dB, $N_b = 25$ dB, and $N_b = 20$ dB. At SNR = 16 dB is the turning point, at SNR<16 dB, both adaptive power transfer outperforms the conventional ATD communication technique, and the cascaded LPF and RNN adaptive power transfer techniques perform better. At SNR > 16 dB, both adaptive power transfer techniques gradually stabilize and reach optimal performance. The adaptive power transfer performance decreases as the background noise gradually increases and the channel reciprocity $\rho < 0.8$. $N_b = 15$ dB shows that the BER performance of the joint LPF and RNN adaptive power transfer techniques is better than that of the LPF-based APT. Meanwhile, in the case of $N_b = 10$ dB and $N_b = 5$ dB, the adaptive power transfer technique performs poorly due to the fact that the reciprocity index is too affected by the background noise in the bidirectional channel.

Figure 8 shows the performance of the five communication techniques in the turbulence condition of $\sigma^2 = 0.1002$. It is evident that the performance has improved at $\rho > 0.9722$, i.e., at the two conditions where the background noise is $N_b = 30$ dB and $N_b = 25$ dB. Taking SNR = 16 dB as the cut-off point, when SNR < 16 dB, the adaptive power transfer technique performs well compared to the traditional ATD technique BER; when SNR > 16 dB, the three adaptive power transfer techniques gradually tend to stabilize and reach the optimal performance value. With the gradual increase of background noise, the signal is flooded by noise and the transmission is affected when the channel reciprocity $\rho < 0.9722$.

Figure 9 shows the performance of the five communication techniques for the turbulence condition of $\sigma^2 = 0.2080$. It is evident that the performance has gotten better at $\rho > 0.8615$, i.e., at three conditions where the background noise is $N_b = 30$ dB, $N_b = 25$ dB, and $N_b = 20$ dB. Taking SNR = 16 dB as the cut-off point, at SNR < 16 dB, the cascaded LPF and RNN adaptive power transfer techniques significantly outperform other adaptive power transfer techniques as well as the conventional ATD technique, whereas the GRU-based and LPF-based adaptive power transfer techniques outperform the FTD technique as the increase in the background noise and the decrease in the intermodulation leads to a similar performance as the conventional ATD technique. At SNR > 16 dB, the three adaptive power transfer techniques gradually level off and reach the performance optimum. With the gradual increase of background noise and channel reciprocity $\rho < 0.8615$, the two techniques

Figure 6
Performance of the signal in the time domain as it moves through $\sigma^2 = 0.1002$'s turbulent channel with varying backgrounds: (a) $N_b = 30$ dB, (b) $N_b = 25$ dB, (c) $N_b = 20$ dB, (d) $N_b = 15$ dB, (e) $N_b = 10$ dB, and (f) $N_b = 05$ dB

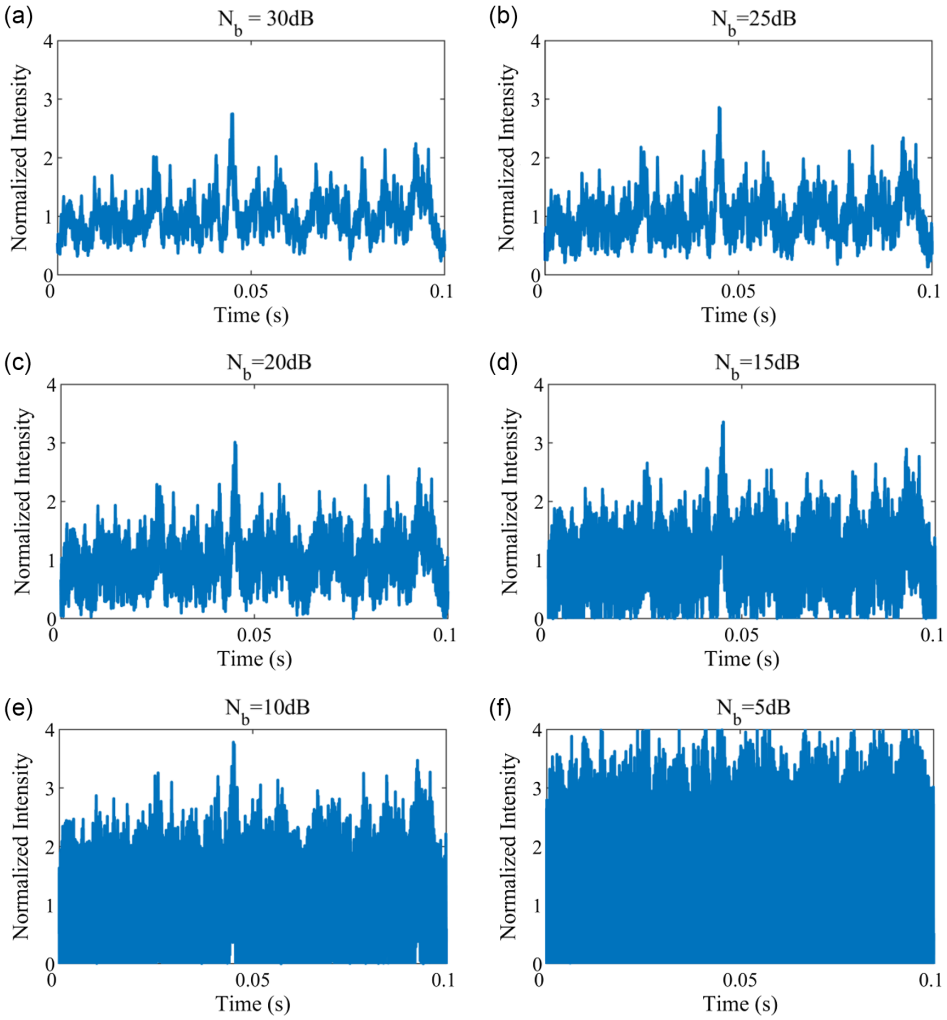

Table 3
Average of three-channel reciprocity measurements under three turbulent channels with different background noises added

N_b(dB)	30	25	20	15	10	05
$\sigma^2 = 0.0596$	0.9912	0.9730	0.9215	0.9214	0.5999	0.3884
$\sigma^2 = 0.1002$	0.9945	0.9831	0.9493	0.8615	0.6903	0.4735
$\sigma^2 = 0.2080$	0.9979	0.9936	0.9804	0.9417	0.8441	0.6630

Table 4
The main parameters of neural network training process

Experimental parameter	Parameter setting	Experimental parameter	Parameter setting
Number of training samples	1×10^7	Batch size	8
Number of verification samples	8×10^6	Optimizer	Adam
Number of testing samples	2×10^6	Loses function	MSE
Data Rate	10 Mbps	Initial learning rate	0.005
SNR range	4–28 dB	Epoch	40
Turbulence intensity	0.0596、0.1002、0.2080	System environment	NVIDIA GeForce RTX 4060 8GB GDDR6

Figure 7
Performance of five transmission techniques in $\sigma^2 = 0.0596$ channel with various noise backgrounds: (a) $N_b = 30$ dB, (b) $N_b = 25$ dB, (c) $N_b = 20$ dB, (d)$N_b = 15$ dB, (e) $N_b = 10$ dB, and (f) $N_b = 05$ dB

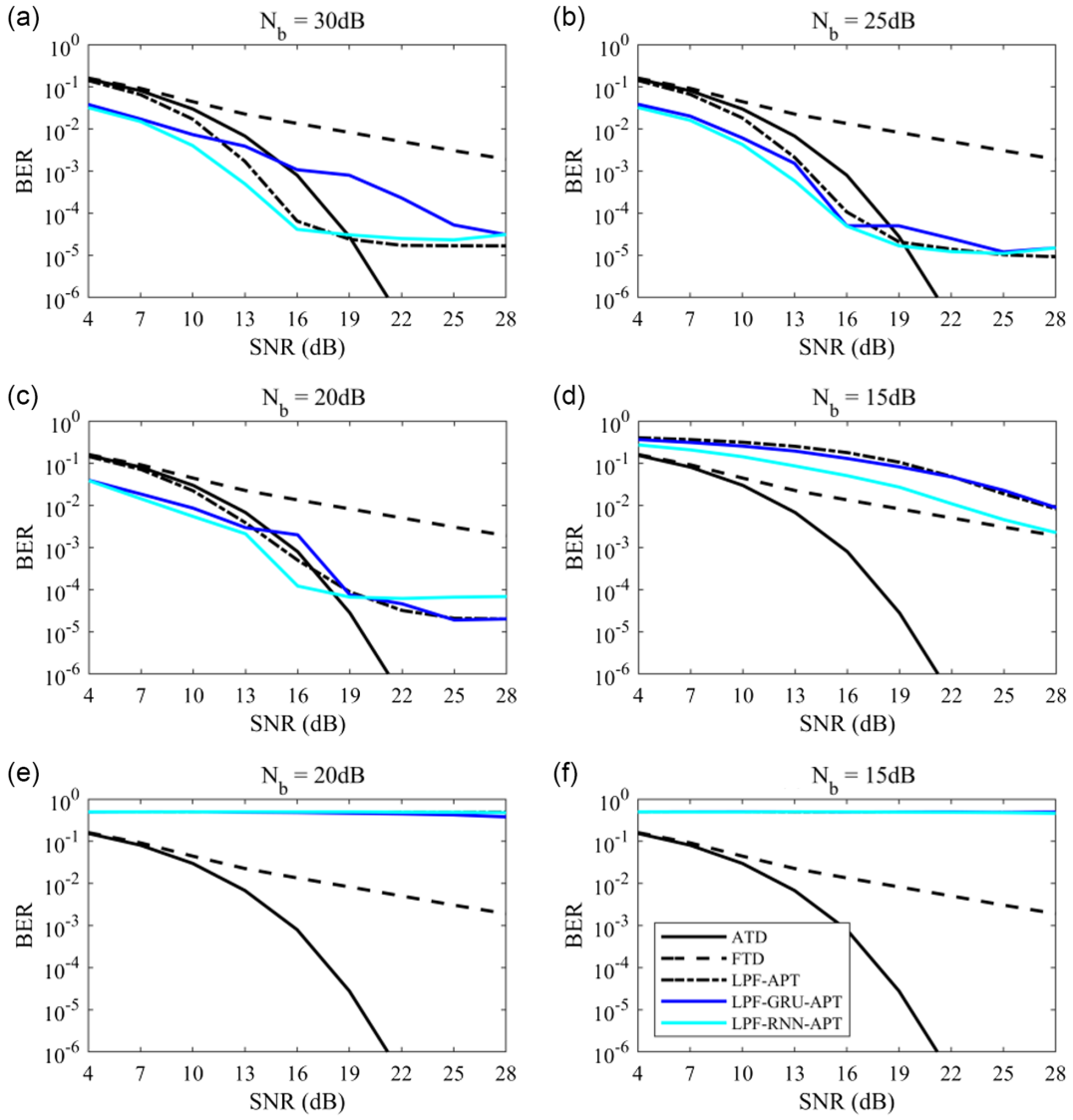

are in the same situation as in Figure 7. And in deep learning models, the root mean squared error (RMSE) is commonly used as the evaluation criterion for regression prediction problems. The RMSE and the operation time of this paper are shown in Table 5.

Figure 10 illustrates the BER performance comparison of different transmission technologies through three turbulent channels under 25 dB conditions. From Figure 10, it can be observed that under conditions with relatively low background noise, the two APT technologies proposed in this work, which incorporate deep learning under reciprocal channel conditions, outperform traditional FTD and ATD technologies, with their BER being an order of magnitude lower. The best performances achieved using the GRU model and the RNN model are represented by 1.1×10^{-5} and 1.03×10^{-5}, respectively. Additionally, after smoothing high-frequency noise using LPF, the BER across the three turbulent channels can be stabilized within the range of $10^{-4} \sim 10^{-5}$.

When the channel scintillation coefficient is fixed, the LPF-RNN-APT technology exhibits a differentiated characteristic in the noise scenarios. In a high-noise environment, which is in the case of relatively low reciprocity, its sequential modeling ability based on the RNN can effectively capture the dynamic correlations of the noise. Combined with the suppression of high-frequency noise by the LPF, a dual noise reduction link is formed, which includes noise trajectory tracking and frequency-domain screening. However, in a low-noise scenario, the advantages of this technology are weakened instead. However, the APT technologies using the GRU and RNN models exhibit similar characteristics under the same experimental conditions: they show an advantage when there is a certain degree of loss in reciprocity. The difference lies in their different degrees of response under the same circumstances, with the LPF-GRU-APT technology having a greater degree of response. There may be two reasons for the comparison between the two.

Figure 8
Performance of five transmission techniques in $\sigma^2 = 0.1002$ channel with various noise backgrounds: (a) $N_b = 30$ dB, (b) $N_b = 25$ dB, (c) $N_b = 20$ dB, (d) $N_b = 15$ dB, (e) $N_b = 10$ dB, and (f) $N_b = 05$ dB

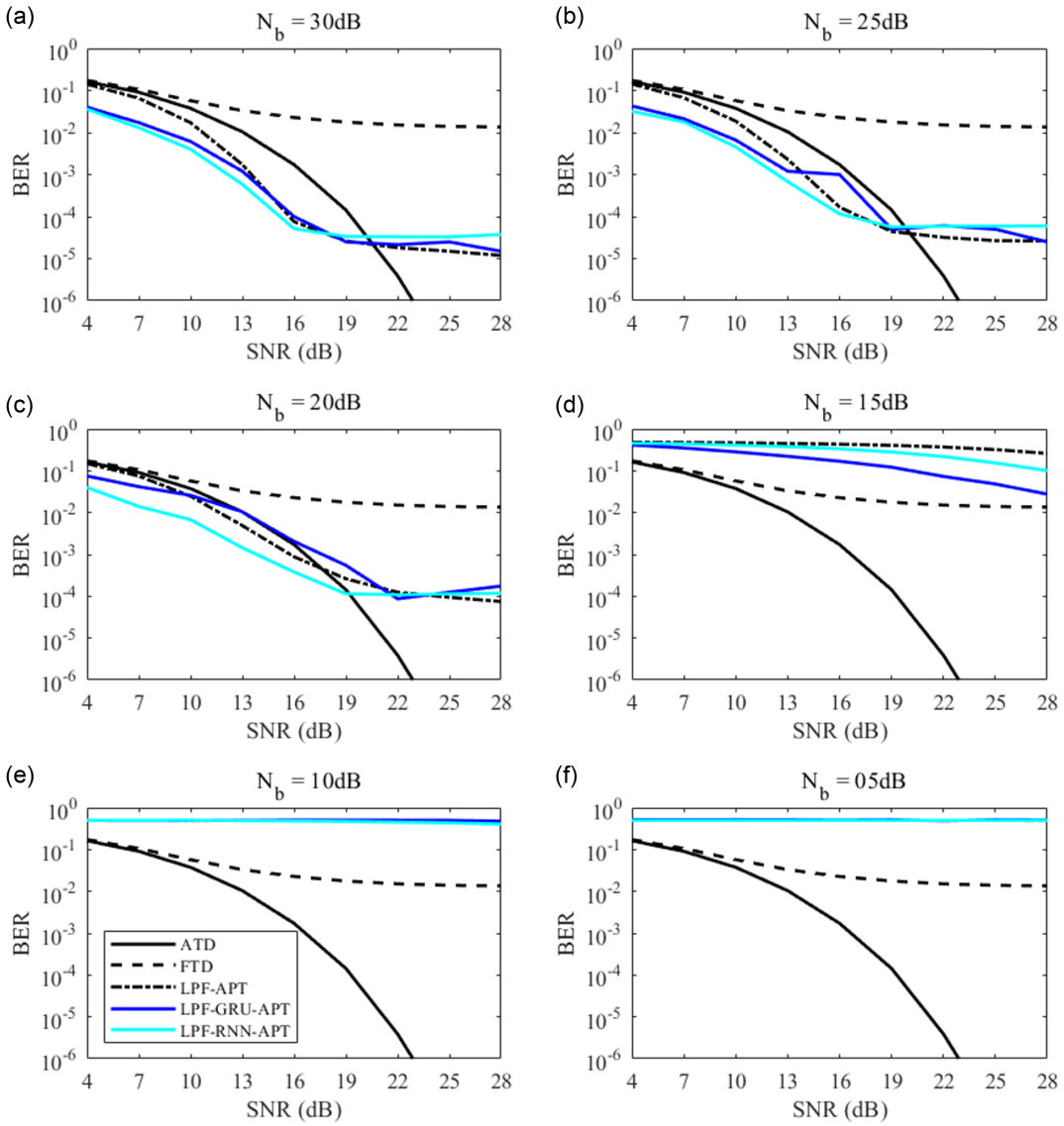

Firstly, it is about the structural complexity. The GRU model has an update gate and a reset gate, and its structure is relatively complex. In a relatively stable environment such as a reciprocal channel, the complex structure is prone to overfitting. In contrast, the RNN has a simple structure. When processing stable data, it will not introduce excessive unnecessary calculations and parameter adjustments and can learn data features more efficiently. Secondly, it is related to the information processing method. The gating mechanism of the GRU will screen and update the information. In a reciprocal channel, this mechanism may excessively change or discard useful information. The RNN, on the other hand, simply circulates and transmits information, which can better preserve the original features and patterns of the data, thus being conducive to the performance of the model.

The experiment reveals that in practical applications of the reciprocity-based APT technology, there exists a complex balancing relationship among reciprocity, the channel scintillation coefficient, and the performance of the deep learning model. Through experimental analysis, it is found that the mutual influence of these parameters directly determines the energy efficiency and transmission stability of the system. Future research will focus on further quantifying the relationships among these parameters by processing a large amount of real-time channel data and conducting simulation experiments, and attempting to find specific numerical ranges as optimization targets. Especially under different conditions of the scintillation coefficient and reciprocity, the performance of the deep learning model varies significantly. Systemic experiments are needed to determine the optimal model structure and parameter configuration, so as to ultimately achieve an efficient and reliable APT scheme.

According to the simulation content, it can be seen that the better the performance of adaptive transmission power technology in the case of turbulent channel scintillation coefficient is small, and the bidirectional atmospheric channel reciprocity is $\rho > 0.8615$. In the case of larger turbulence

Figure 9
Performance of five transmission techniques in $\sigma^2 = 0.2080$ channel with various noise backgrounds: (a) $N_b = 30$ dB, (b) $N_b = 25$ dB, (c) $N_b = 20$ dB, (d) $N_b = 15$ dB, (e) $N_b = 10$ dB, and (f) $N_b = 05$ dB

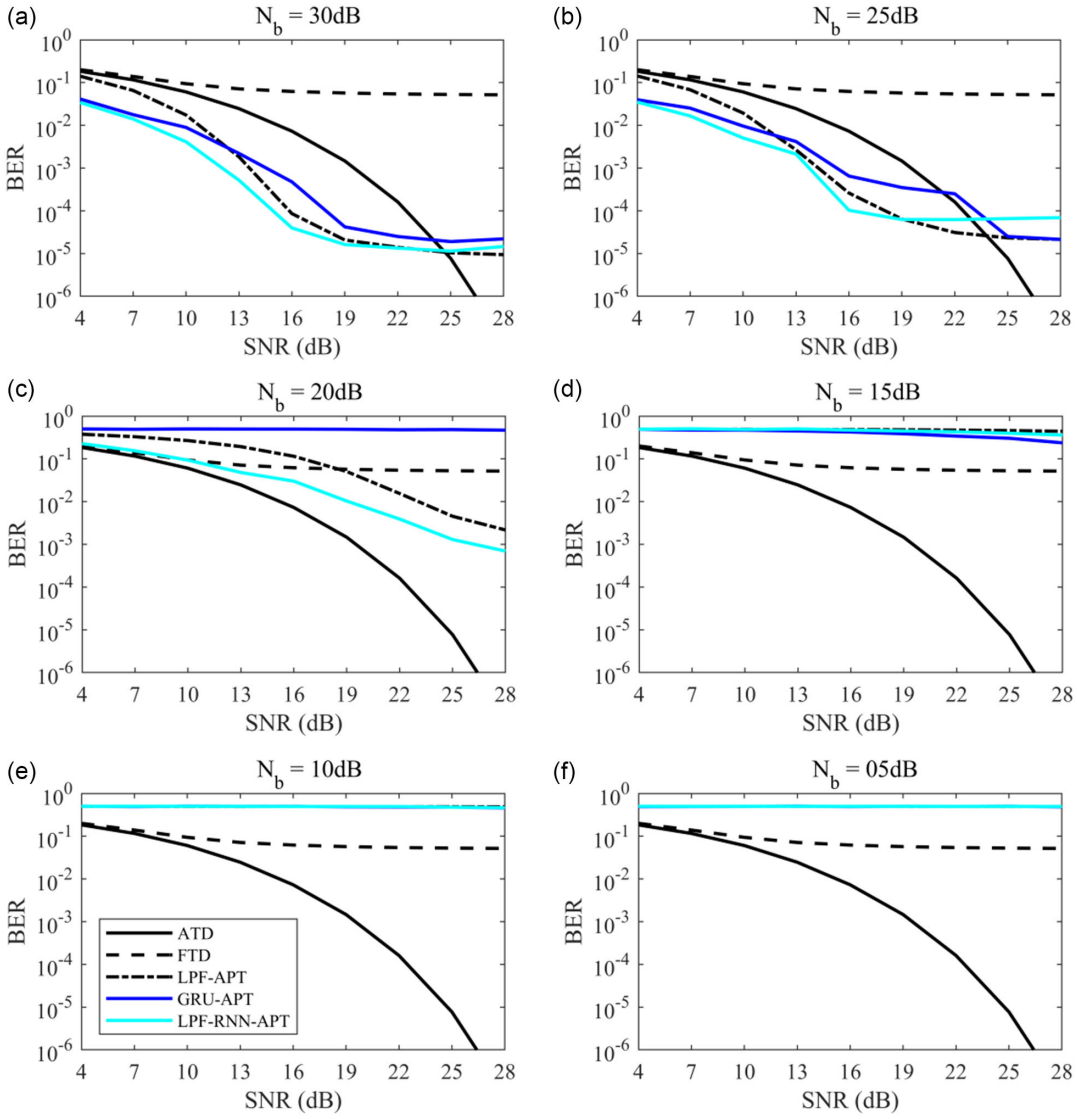

Table 5
RMSE and training time of the two techniques in different turbulent channels in $N_b = 30$ dB

Deep learning model	Optimizer	Turbulence intensity	RMSE	Training time
GRU	Adam	0.0596	0.1362	414 s
		0.1002	0.1425	425 s
		0.2080	0.1225	462 s
RNN	Adam	0.0596	0.0472	256 s
		0.1002	0.0351	251 s
		0.2080	0.0551	255 s

coefficients, the adaptive transmission technique requires more accurate channel reciprocity, and in turbulence channel $\sigma^2 = 0.2080$, the channel reciprocity is required to be $\rho > 0.9722$. Both adaptive transmission techniques based on deep learning outperform traditional FTD and ATD technologies. The introduction of LPF reduces high-frequency noise, stabilizing the BER floor within a certain range $10^{-4} \sim 10^{-5}$ at high SNR conditions. In summary, in reciprocal APT FSO systems, RNN stands out due to its lightweight structure and parameter efficiency, demonstrating exceptional performance in strongly symmetric channels and suitability for real-time power control. This advancement extends the practical application of adaptive power control algorithms in complex atmospheric environments.

Figure 10
BER performance of different transmission technologies under three kinds of turbulence at 25 dB

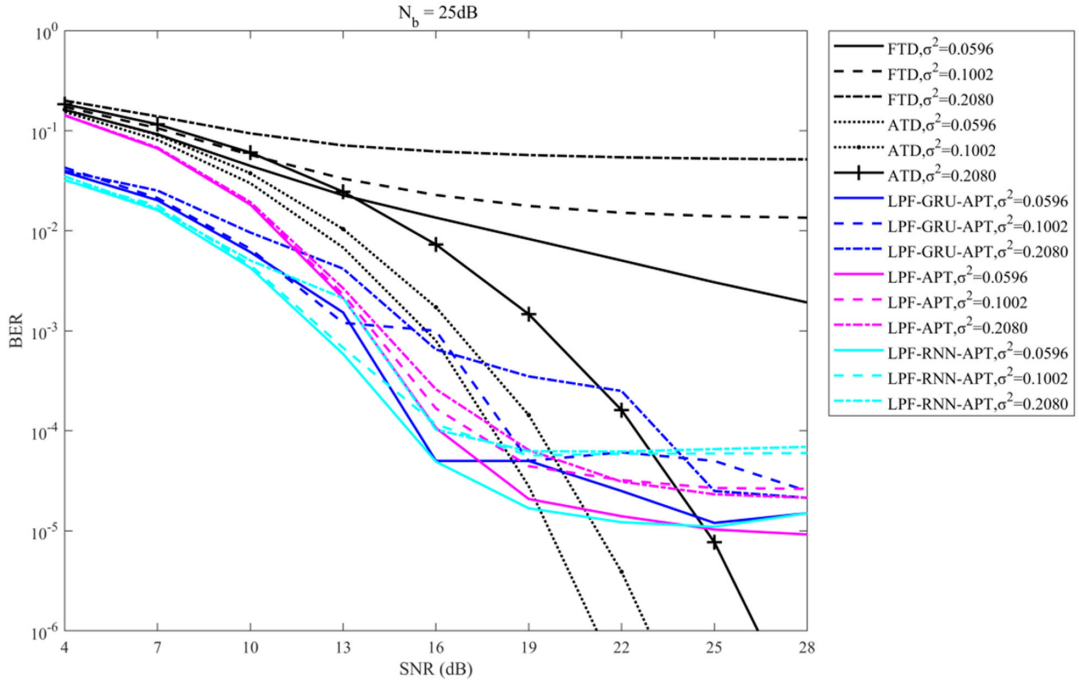

5. Conclusion

This paper proposes two distinct APT systems for FSO communication systems based on the reciprocity of bidirectional channels: the LPF-RNN-APT technology and the LPF-GRU-APT technology. The effectiveness of these methods has been validated through simulations. The results indicate that, compared to traditional techniques, the APT technologies proposed in this study can achieve a lower bound that stabilizes within $10^{-4} \sim 10^{-5}$ in highly reciprocal turbulent channels. Specifically, the LPF-RNN-APT technology excels due to its lightweight structure and parameter efficiency, demonstrating outstanding performance in strongly symmetric channels. The proposed APT technologies effectively compensate for turbulence, enhancing the BER performance of the signal and mitigating the impact of atmospheric turbulence-induced scintillation effects on FSO communication systems.

Ethical Statement

This study does not contain any studies with human or animal subjects performed by any of the authors.

Conflicts of Interest

The authors declare that they have no conflicts of interest to this work.

Data Availability Statement

Data are available on request from the corresponding author upon reasonable request.

Author Contribution Statement

Wen-Yao Liu: Investigation, Resources, Data curation, Writing – original draft, Visualization. **Yan-Qing Hong:** Conceptualization, Methodology, Validation, Formal analysis, Writing – review & editing, Supervision, Project administration. **Xu Liu:** Software, Validation, Resources. **Xue-Heng Chen:** Data curation, Writing – review & editing. **Peng-Fei Lv:** Formal analysis, Writing – review & editing.

References

[1] Al-Gailani, S. A., Mohd Salleh, M. F., Salem, A. A., Shaddad, R. Q., Sheikh, U. U., Algeelani, N. A., & Almohamad, T. A. (2021). A survey of free space optics (FSO) communication systems, links, and networks. *IEEE Access*, *9*, 7353–7373. https://doi.org/10.1109/ACCESS.2020.3048049

[2] Kaushal, H., & Kaddoum, G. (2017). Optical communication in space: Challenges and mitigation techniques. *IEEE Communications Surveys & Tutorials*, *19*(1), 57–96. https://doi.org/10.1109/COMST.2016.2603518

[3] Khalid, H., Sajid, S. M., Nistazakis, H. E., & Ijaz, M. (2024). Survey on limitations, applications and challenges for machine learning aided hybrid FSO/RF systems under fog and smog influence. *Journal of Modern Optics*, *71*(4–6), 101–125. https://doi.org/10.1080/09500340.2024.2402428

[4] Huang, Y., Huang, H., Chen, H., Alvarado, J. C., Zhang, Q., Fontaine, N. K., …, & Wang, M. (2021). Elliptical-aperture multimode diversity reception for free-space optics communications under anisotropic turbulence. In *Optical Fiber Communication Conference*, W7E.4. https://doi.org/10.1364/OFC.2021.W7E.4

[5] Khalighi, M. A., & Uysal, M. (2014). Survey on free space optical communication: A communication theory perspective. *IEEE Communications Surveys & Tutorials*, *16*(4), 2231–2258. https://doi.org/10.1109/COMST.2014.2329501

[6] Maalej, M., & Besbes, H. (2020). Performance of free space optical communication system based on M-ary PPM modulation over

double generalized gamma channel. *China Communications*, *17*(4), 19–30. https://doi.org/10.23919/JCC.2020.04.003

[7] Campos, A. C., Georgieva, P., Fernandes, M. A., Monteiro, P. P., Fernandes, G. M., & Guiomar, F. P. (2024). Optical beam steering in FSO systems supported by computer vision. *IEEE Access*, *12*, 73793–73809. https://doi.org/10.1109/ACCESS.2024.3405196

[8] Hufnagel, F., Sit, A., Grenapin, F., Bouchard, F., Heshami, K., England, D., . . . , & Karimi, E. (2019). Characterization of an underwater channel for quantum communications in the Ottawa River. *Optics Express*, *27*(19), 26346–26354. https://doi.org/10.1364/OE.27.026346

[9] Cozzolino, D., da Lio, B., Bacco, D., & Oxenløwe, L. K. (2019). High-dimensional quantum communication: Benefits, progress, and future challenges. *Advanced Quantum Technologies*, *2*(12), 1900038. https://doi.org/10.1002/qute.201900038

[10] Liu, W., Chen, X., Liu, M., & Hong, Y. (2023). Bidirectional atmospheric channel reciprocity-based adaptive power transmission. *Photonics*, *10*(10), 1067. https://doi.org/10.3390/photonics10101067

[11] LeCun, Y., Bengio, Y., & Hinton, G. (2015). Deep learning. *Nature*, *521*(7553), 436–444. https://doi.org/10.1038/nature14539

[12] Padhy, J. B., & Patnaik, B. (2018). Multiplexed free-space optical system design using Manchester coding. *Optik*, *174*, 266–273. https://doi.org/10.1016/j.ijleo.2018.07.140

[13] Kaur, S., & Lubana, A. (2024). Performance investigation of Ro-FSO link under clear and fog conditions employing machine learning. *Journal of Optics*. Advance online publication. https://doi.org/10.1007/s12596-024-01904-z

[14] Shao, W., Wang, Y., Jia, S., Xie, Z., Gao, D., Wang, W., . . . , & Xie, X. (2022). Terabit FSO communication based on a soliton microcomb. *Photonics Research*, *10*(12), 2802–2808. https://doi.org/10.1364/PRJ.473559

[15] Amirabadi, M. A., Kahaei, M. H., Nezamalhosseini, S. A., & Vakili, V. T. (2020). Deep learning for channel estimation in FSO communication system. *Optics Communications*, *459*, 124989. https://doi.org/10.1016/j.optcom.2019.124989

[16] Shapiro, J. H. (1971). Reciprocity of the turbulent atmosphere. *Journal of the Optical Society of America*, *61*(4), 492–495. https://doi.org/10.1364/JOSA.61.000492

[17] Ip, E., & Kahn, J. M. (2006). Power spectra of return-to-zero optical signals. *Journal of Lightwave Technology*, *24*(3), 1610–1618. https://doi.org/10.1109/JLT.2005.863328

[18] Elsayed, E. E. (2024). Investigations on OFDM UAV-based free-space optical transmission system with scintillation mitigation for optical wireless communication-to-ground links in atmospheric turbulence. *Optical and Quantum Electronics*, *56*(5), 837. https://doi.org/10.1007/s11082-024-06692-1

[19] Liu, N., Zhong, W. D., He, Y., Heng, K. H., & Cheng, T. H. (2008). Comparison of NRZ and RZ modulations in laser intersatellite communication systems. In *Proceedings of the 2008 International Conference on Advanced Infocomm Technology*, *55*, 1–4. https://doi.org/10.1145/1509315.1509370

[20] Lv, P. F., & Hong, Y. Q. (2023). Self-pilot tone based adaptive threshold RZ-OOK decision for free-space optical communications. *Photonics*, *10*(7), 714. https://doi.org/10.3390/photonics10070714

[21] Chen, J., Huang, Y., Cai, R., Zheng, A., Yu, Z., Wang, T., . . . , & Gao, S. (2020). Free-space communication turbulence compensation by optical phase conjugation. *IEEE Photonics Journal*, *12*(5), 7905611. https://doi.org/10.1109/JPHOT.2020.3024220

[22] Wang, X., Wu, T., Dong, C., Zhu, H., Zhu, Z., & Zhao, S. (2021). Integrating deep learning to achieve phase compensation for free-space orbital-angular-momentum-encoded quantum key distribution under atmospheric turbulence. *Photonics Research*, *9*(2), B9–B17. https://doi.org/10.1364/PRJ.409645

[23] Mansour Abadi, M., Ghassemlooy, Z., Khalighi, M. A., Zvanovec, S., & Bhatnagar, M. R. (2016). FSO detection using differential signaling in outdoor correlated-channels condition. *IEEE Photonics Technology Letters*, *28*(1), 55–58. https://doi.org/10.1109/LPT.2015.2480011

[24] Ding, S., Zhang, J., & Dang, A. (2017). Adaptive threshold decision for on-off keying transmission systems in atmospheric turbulence. *Optics Express*, *25*(20), 24425–24436. https://doi.org/10.1364/OE.25.024425

[25] Elganimi, T. Y. (2013). Performance comparison between OOK, PPM and PAM modulation schemes for free space optical (FSO) communication systems: Analytical study. *International Journal of Computer Applications*, *79*(11), 22–27. https://doi.org/10.5120/13786-1838

[26] Bhowal, A., & Kshetrimayum, R. S. (2019). Transmit laser selection for two hop decode and forward FSO communication with pointing errors. *IEEE Communications Letters*, *23*(12), 2301–2305. https://doi.org/10.1109/LCOMM.2019.2942309

[27] Riediger, M. L. B., Schober, R., & Lampe, L. (2008). Blind detection of on-off keying for free-space optical communications. In *Canadian Conference on Electrical and Computer Engineering*, 001361–001364. https://doi.org/10.1109/ccece.2008.4564763

[28] Elsayed, E. E. (2024). Atmospheric turbulence mitigation of MIMO-RF/FSO DWDM communication systems using advanced diversity multiplexing with hybrid N-SM/OMI M-ary spatial pulse-position modulation schemes. *Optics Communications*, *562*, 130558. https://doi.org/10.1016/j.optcom.2024.130558

[29] Palitharathna, K. W. S., Suraweera, H. A., Godaliyadda, R. I., Herath, V. R., & Thompson, J. S. (2021). Average rate analysis of cooperative NOMA aided underwater optical wireless systems. *IEEE Open Journal of the Communications Society*, *2*, 2292–2310. https://doi.org/10.1109/OJCOMS.2021.3116146

[30] Yousif, B. B., & Elsayed, E. E. (2019). Performance enhancement of an orbital-angular-momentum-multiplexed free-space optical link under atmospheric turbulence effects using spatial-mode multiplexing and hybrid diversity based on adaptive MIMO equalization. *IEEE Access*, *7*, 84401–84412. https://doi.org/10.1109/ACCESS.2019.2924531

How to Cite: Liu, W.-Y., Hong, Y.-Q., Liu, X., Chen, X.-H., & Lv, P.-F. (2025). Deep Learning Model-Based Adaptive Power Transfer in FSO Communications. *Journal of Optics and Photonics Research*. https://doi.org/10.47852/bonviewJOPR52024929